Marine Geology 271 (2010) 119–130

Contents lists available at ScienceDirect

Marine Geology

journal homepage: www.elsevier.com/locate/margeo

Quantifying tidal signatures of the benthic nepheloid layer in Gaoping Submarine Canyon in Southern Taiwan

James T. Liu [a,*], Yu Huai Wang [b], I-Huan Lee [c], Ray T. Hsu [d]

[a] Institute of Marine Geology and Chemistry, National Sun Yat-sen University, Kaohsiung Taiwan 804-24, ROC
[b] Institute of Applied Marine Physics and Undersea Technology, National Sun Yat-sen University, Kaohsiung Taiwan 804-24, ROC
[c] National Museum of Marine Biology and Aquarium, Pingtung Taiwan 94450, ROC
[d] Institute of Marine Geology and Chemistry, National Sun Yat-sen University, Kaohsiung Taiwan 804-24, ROC

ARTICLE INFO

Article history:
Received 4 August 2009
Received in revised form 8 January 2010
Accepted 23 January 2010
Available online 10 February 2010

Communicated by G.J. de Lange

Keywords:
submarine canyon
suspended sediment
particle size
benthic nepheloid layer (BNL)
internal tide
nonlinearity

ABSTRACT

The benthic nepheloid layer (BNL) has been observed in the head region of the Gaoping/Kaoping Submarine Canyon (KPSC) throughout a year. The top of the BNL could be as high as 100 m above the canyon floor in which the suspended sediment concentration (SSC) could be as high as 30 mg/l. In the BNL, sand-sized particles comprise the largest size-class in the suspended sediment population.

Based on three one-month time series observations near the canyon floor of along-canyon velocity, water temperature, and the volume concentration (VC) of clay, very-fine-to-medium silt, coarse silt and sand size-classes in 2000, 2002, and 2004, the BNL is strongly modulated by the tides at semidiurnal, diurnal, quarter, and sixth diurnal and spring-neap frequencies. In the course of a semidiurnal tidal cycle, the flood (up-canyon) current brings colder water from the seaward part of the canyon causing the SSC and the thickness of the BNL to increase. The SSC immediately near the canyon floor also increases in response to the maximum flood and ebb currents of the M_2 tide.

The tidal-to-total energy ratio (ER) of the along-canyon flow is between 70–80%, and between 50–80% among the suspended sediment of clay, very-fine-to-medium silt, coarse silt and sand size-classes. The M_2 is the most important tidal constituent in the temporal variations of along-canyon flow, water temperature, and the VC of the four size-classes. The local phase differences between the forcing (velocity), and the responses (temperature and VC) at the M_2 frequency show distinct phase-lock that suggests patterns of standing and progressive internal tides. Suspended sediments in the BNL also respond to the M_2 forcing in a coherent fashion.

Suspended sediment movements are strongly affected by nonlinear processes as indicated by the elevated values of the amplitude ratio of M_4/M_2 of the suspended sediment size-classes comparing to that of the flow. The cross-canyon geometry and the slope of the submarine canyon floor affect the propagation of the barotropic and internal tides, which in turn, affect the nonlinearity generation in the BNL.

1. Introduction

The benthic nepheloid layer (BNL) has been widely observed in many different marine and oceanographic settings. These settings include open continental shelves (Inthorn et al., 2006; McCave and Hall, 2002; Oliveira et al., 2002; van der Loeff et al., 2002; Vitorino et al., 2002; van Weering, et al., 2001), marginal seas (Chronis et al., 2000; Karageorgis and Anagnostou, 2001; Ramaswamy et al., 2004; Yurkovskis, 2005; Zhu et al., 2006), and submarine canyons (Frignani, et al., 2002; Liu et al., 2002; Puig and Palanques, 1998; Puig et al., 2004).

The BNL on the shelf is maintained by resuspension of the bottom sediment by waves and tidal currents (Chronis et al., 2000; Karageorgis and Anagnostou, 2001; Ramaswamy et al., 2004; van der Loeff et al., 2002; van Weering et al., 2001). Sediment in the BNL is often transported over the shelf edge/break (Forest et al., 2007) following isopycnal surfaces and form the intermediate nepheloid layer (INL) over the slope (McCave et al., 2001; McCave and Hall, 2002; McPhee-Shaw et al., 2004; Oliveira et al., 2002).

In shallow waters, processes related to the breaking of internal waves affect the movement of the suspended sediment in the BNL (Chronis et al., 2000; Johnson et al., 2001). Internal tides have a much wider influence on the resuspension and advection of the suspended sediment in the BNL over continental shelves, slopes, and in submarine canyons (Puig et al., 2001, 2004; Ribbe and Holloway, 2001). On some occasions, sediment is transported from the adjacent shelf to submarine canyons via the BNL (Frignani, et al., 2002; Oliveira et al., 2007). High mass fluxes measured in the BNL in submarine canyons (Liu et al., 2006, 2009a; van Weering et al., 2001) suggest that major sediment transport and rapid accumulation occur in the BNL in

* Corresponding author. Tel.: +886 7 525 5144; fax: +886 7 525 5130.
E-mail address: james@mail.nsysu.edu.tw (J.T. Liu).

0025-3227/$ – see front matter © 2010 Elsevier B.V. All rights reserved.
doi:10.1016/j.margeo.2010.01.016

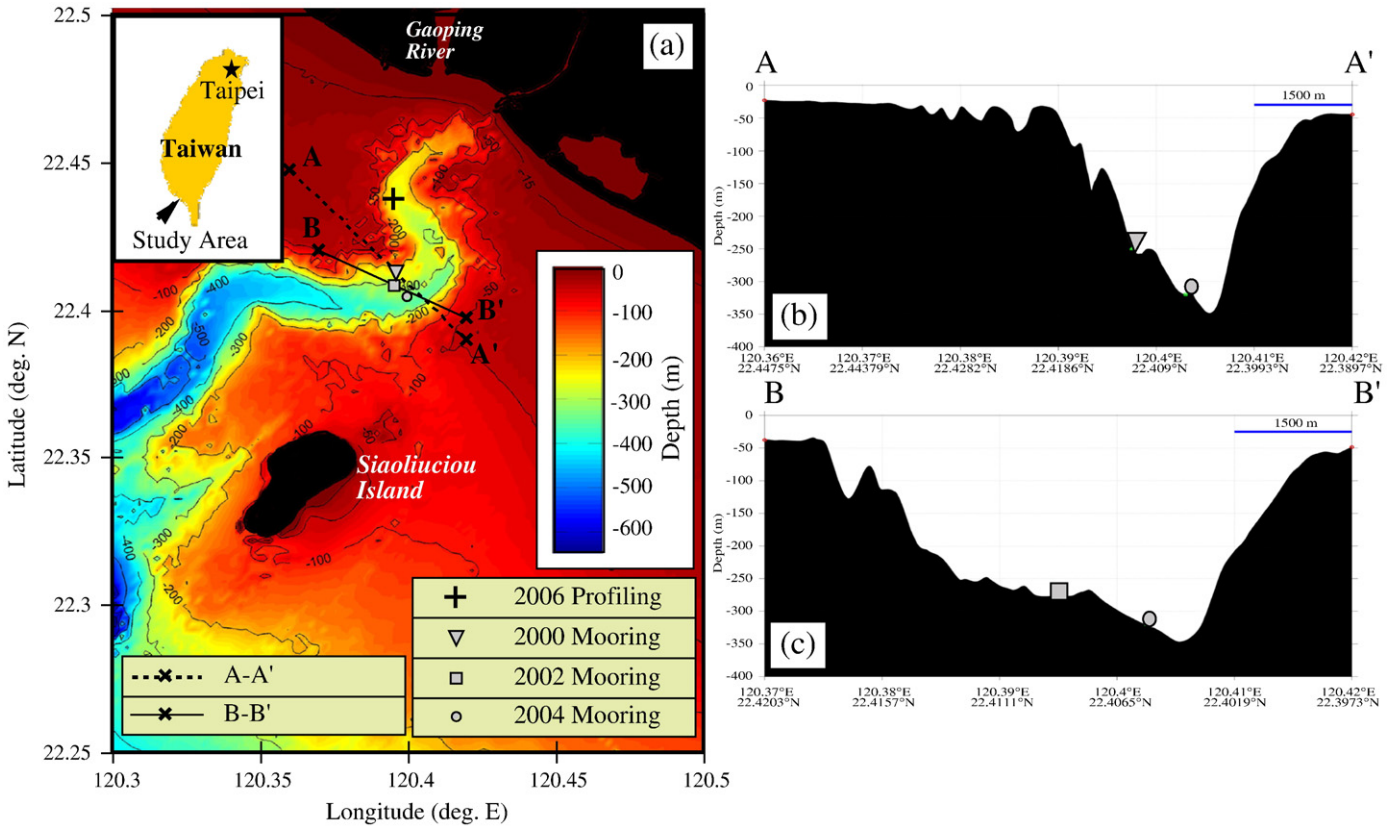

Fig. 1. (a) Map showing the deployment sites of the sediment trap moorings in 2000, 2002, and 2004, respectively in the head region of the Gaoping Submarine Canyon (KPSC); and the 25-h profiling station in the head region of the canyon in 2006. (b) Line A–A′ shows the water depth of a perpendicular cross-section encompasses the locations of 2000 and 2004 moorings. (c) Line B–B′ shows a slanted cross-section that encompasses the locations of 2002 and 2004 moorings. The insert is a larger-scaled map showing the island of Taiwan.

submarine canyons and the BNL is significant in the submarine canyon conduit to supply sediment to the deeper part of the ocean basin (Liu et al., 2009a; Masque et al., 2003).

Internal tides could be generated at the canyon opening, the rim, and along the canyon floor (Kunze et al., 2002; Petruncio et al., 2002), and propagate up-canyon with enhanced bottom currents. In addition to the tidal current, the temperature, turbidity and suspended sediment concentration (SSC) observed in submarine canyons also fluctuate predominantly at semidiurnal tidal frequencies in the BNL (Liu and Lin, 2004; Liu et al., 2006; Puig et al., 2004). These fluctuations together with the density characteristics of submarine canyons suggest that internal tides are important mechanisms affecting the BNL in the canyon. However, there have not been many studies on the quantitative link between the BNL and internal tidal forcing in submarine canyons. Therefore, the objective of this study is to quantify the tidal characteristics of the along-canyon flow, water temperature, and the concentrations of different grain-size-classes of suspended sediment in the BNL in order to understand how internal tides affect the BNL in a submarine canyon conduit.

2. Study area and background

A multidisciplinary research program called '*Fa*te of the *te*rrestrial substances in the Gaoping (formally spelled Kaoping) Submarine Canyon' (FATES-KP) has been investigating the source, pathway, transport, and fate of sediments in a river-sea system consisting of a small mountainous river (Gaoping River, KPR) and the adjacent Gaoping Submarine Canyon (KPSC) off Southern Taiwan (Liu et al., 2009b). KPSC is a two-way conduit for the transport of terrestrial sediment and particles of marine origins (Liu et al, 2006, Liu et al., 2009a). The water column in the interior of the KPSC is stratified primarily due to strong temperature gradients (Liu et al., 2002; Lee et al., 2009a,b). Both barotropic and baroclinic tides are strong in the canyon and have equal magnitudes (Lee et al., 2009a). The tidal current velocity and water temperature in the canyon are dominated by semidiurnal tides yet diurnal and higher harmonics are also significant (Lee et al., 2009a,b). The amplitude of tidal velocity and vertical phase shift in the canyon increase with depth and increase toward the canyon head (Wang et al., 2008). In the head region of the canyon, tidal flows are up-canyon directed during the flood and down-canyon directed during the ebb. The up-canyon flood flow also brings colder water from offshore toward the canyon head (Wang et al., 2008; Lee et al., 2009a,b).

The existence of isopycnal surfaces in the canyon is conducive to the propagation of internal tides and the existence of a critical bottom slope in the head region of KPSC also favors the generation of internal tides (Lee et al., 2009a; Liu et al., 2002; Wang et al., 2008). From observed temporal changes of velocity and density profiles, the 1st two modes of semidiurnal internal tide are resolved (Lee et al., 2009a,b). The headward propagation of the internal tidal wave is analogous to a beam parallel to the bottom topography of the canyon (Wang et al., 2008). This scenario is consistent with the vertical displacement of isopycnal depth (isotherms) on the order of 160 m due to the advection of colder water in the course of a semidiurnal tidal cycle (Lee et al., 2009a; Wang et al., 2008). The internal tidal energy (depth integrated baroclinic tidal

Table 1
The height of each instrument above the sea floor on the tree taut-line moorings.

Year	Water depth (m)	Instrument height (meters above bed)	
		LISST-100	Current meter (type)
2000	290	5	50(rotary)
2002	313	28	33(rotary)
2004	315	41	47(acoustic)

energy) flux in the head region of the KPSC is 3–7 times greater than that found in Monterey Canyon which is likely due to larger (10 times greater) barotropic tide in the KPRSC (Lee et al., 2009a).

Since the head of the canyon forms an ultimate terminus for the propagating tide, the complex geometry of the canyon boundaries, and the existence of a super critical bottom slope near the canyon head, standing semidiurnal internal tides have been observed. The characteristics of the 1st mode standing wave has the 90–110° phase lag between the along-canyon velocity and the density interface (Lee et al., 2009b, Wang et al., 2008).

In the head region the substrate surface of the canyon floor is composed of mostly mud (grain size finer than 63 μm), of which the

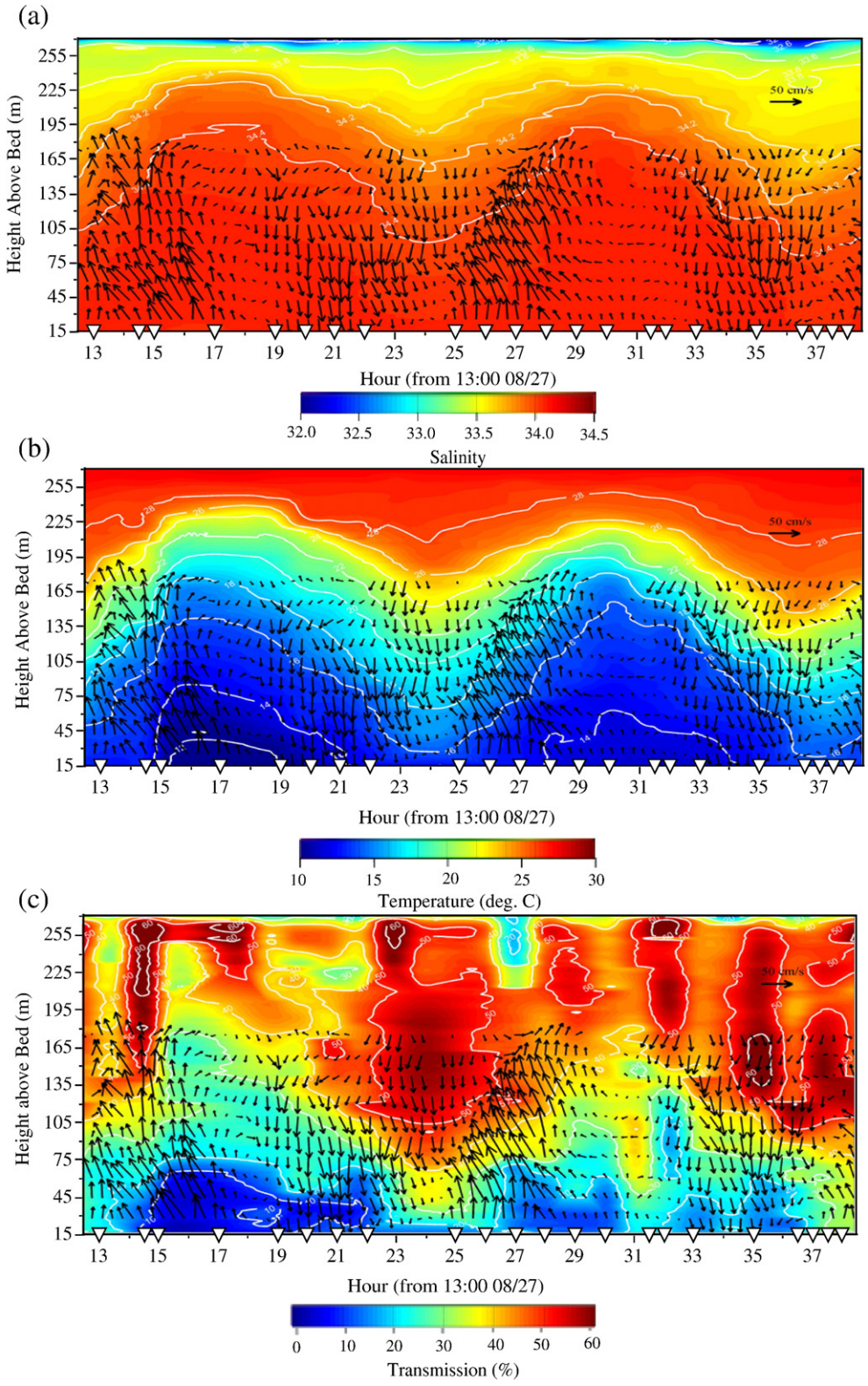

Fig. 2. The result of 25 hourly profiling measurements of salinity (a), temperature (b), light transmission and shipboard ADCP (c) from 13:00 of Aug. 27 to 14:00 of Aug. 28. The arrows indicate the magnitude and horizontal orientation (north is upward) of the flow (c). The inverse triangles indicate the time of 22 LISST profile measurements.

medium- to fine-grained silt size-class dominates (Liu et al., 2002). Previous studies have found that the BNL is present in the KPSC throughout the year (Liu et al., 2002, Lee et al., 2009a). The thickness of the BNL could be greater than 100 m above the canyon floor and the suspended sediment concentration (SSC) in the BNL could exceed 30 mg/l (Liu et al., 2002). Most suspended sediment transport in the KPSC took place within BNL in which mass fluxes of settling sediment measured by sediment traps in the canyon during the energetic typhoon and flood season of the KPR can exceed 800 g/m^2/d (Liu et al., 2009a). Within the BNL, localized pockets of high SSC have a similar length scale of the turbulence overturning suggesting a cause-effective relationship (Lee et al., 2009a). Tide-related processes are the primary mechanism for resuspension and transport of suspension sediment in the KPSC.

3. Field experiments and methods

For observing particle dynamics at a hypothesized depocenter (Liu et al., 2002) sediment trap moorings were deployed for one month at similar locations (Fig. 1) in the head region of the Gaoping Submarine Canyon (Fig. 1) in 2000 (June 20–July 20), 2002 (June 27–July 26), and 2004 (May 26–June 26), respectively (Liu and Lin, 2004; Liu et al., 2006; Lee and Liu, 2006; Liu et al., 2009b). These locations were on the south side of the canyon wall where the canyon axis forms a meandering bend (Fig. 1b, c) whose cross-section is v-shaped (Fig. 1b). The year 2000 mooring was the closest to the canyon wall (Fig. 1b). The 2004 mooring was the closest to the thalweg. The 2002 mooring was located in a relatively open space in the canyon (Fig. 1c). In this paper, we focus on the analyses of simultaneously observed records by a current meter (rotary or acoustic) and a Laser In-situ Scattering and Transmissometry (LISST-100) co-located at similar levels on each mooring (Table 1). All records from the same year are synchronized to have the same beginning and ending times having the sampling interval of 1 h before analysis using harmonic analysis, spectral analysis, and other statistical analysis techniques.

In addition to the moored platforms, hourly hydrographic profiling was conducted over a 25-h period at a location closer to the mouth of the KPR (Fig. 1) on board *R/V Ocean Researcher III* (*OR-3*) on Aug. 27, 2006. The profiling consisted of CTD and light transmission (Sea Bird SBE 9/11), and in-situ volume concentration (VC, in μl/l) of 32 particle sizes using a LISST-100.

4. Results

For a better spatial and temporal perspective of the issue at hand, the changes of vertical structure of the suspended sediment volume concentration (VC) measured by the LISST-100 in the course of two semidiurnal tidal cycles are presented first before the time series observations from moored platforms are presented.

4.1. Tidal variations of the vertical structures of volume concentrations (VC) of suspended sediment

The 25-h hydrographic CTD and transmissometry and LISST-100 records began on 13:00 of Aug. 27 through 14:00 of Aug. 28 (Fig. 2). Because of onboard data download and instrumentation procedure, the LISST-100 record only consists of 22 profiles (Fig. 3). The time points at which a LISST-100 record was obtained are indicated by inverse triangles on the time-axis of the salinity (Fig. 2a), temperature (Fig. 2b), and light transmission (Fig. 2c) plots.

At the surface there was a thin (about 15 m) SNL (surface nepheloid layer) of water having low values of salinity (Fig. 2a) and light transmission (Fig. 2c) indicating the presence of the river plume. Below the depth of 50 m, all the salinity, temperature, light transmission, and currents from shipboard ADCP show distinctive tidal signals (Fig. 2a, b, c). During the flood stage in the deeper part of the canyon, the up-canyon current flowed along the thalweg of the canyon and brought in colder water (Fig. 2b) from offshore (Wang et al., 2008) that also carried higher suspended sediment concentration as indicated by the low light transmission (Fig. 2c). The colder offshore water containing higher SSC could increase the thickness of the BNL by at least 10 s of meters in the course of a semidiurnal tidal cycle (using the height of the 30% light transmission isoline as an indicator, Fig. 2c). However, near the canyon floor high SSC (low values of light transmission) also coincided with strong ebb flow (Fig. 2c).

The LISST profiling data is plotted as cumulative VC (Fig. 3) of the following size-classes: 0–3 (clay), 3–10 (very-fine-to-medium silt), 10–63 (coarse silt), and greater than 63 μm (sand and coarser) based on the mesh size for a nested filtration system of the water samples (subject of another study and results not presented here). The cumulative VC shows not only the total value but also the size-composition in terms of the above 4 size-classes. Since *R/V OR-3* does not have a dynamic positioning system, during each profiling operation, the ship might have drifted slightly. Subsequently, the profiled water depth might not be exactly the same because of the drastic depth change if the ship drifted toward the canyon wall (Fig. 1). Also due to the time constraint by all the sampling tasks at a scheduled sampling time, this drift was not fully corrected on some occasions (Fig. 3). For each profile (expressed as meters above the bed, mab), the cumulative VC is plotted against the temperature, which provides a qualitative indication of the stage of the tide and the vertical density structure. To show the magnitude change during the entire sampling period, the plotting ranges for temperature and VC are fixed except for the time point at 17:00, where the upper bound of the VC had to be increased from 80 to 180 μl/l to accommodate the exceptionally high value in the BNL (Fig. 3). Both the light transmission data and the LISST data show bi-modal distribution of a consistent SNL related to the river plume of the KPR and a BNL at depth related to the tide in the canyon.

The largest size-fraction in the BNL includes particles coarser than 63 μm. Based on the ADCP measurements (Fig. 2c), the profiling period included two full semidiurnal tides of which the first flood half-cycle was roughly between 13:00 and 18:00; and the second flood was between 25:00–30:00 (Fig. 2c). Visual examination of the LISST and temperature plots corroborates with the tidal stage designation. During the flood, the VC values gradually increased and the BNL thickened (Fig. 3). The exceptionally high VC value that occurred at 17:00 (Fig. 3) coincided with the max. up-canyon flow (Fig. 2c). The high VC values on 19:00 might suggest a time lag between the peak flow and peak high suspended sediment concentration. In the second flood half-cycle, the maximum flow coincided with high near-bed VC values and increased BNL thickness on 27:00. During the maximum ebb (22:00 and 36:30), the VC values also increased, yet the thickness of the BNL continued to decrease and the BNL was less conspicuous.

4.2. Simultaneous time series observations by sediment trap moorings

All moored data sets presented in this paper contain monthly measurements of the along-canyon flow, water temperature and the VC of the same four size-classes near the canyon floor (Table 1, Figs. 4–6). The tidal signal of each time series was quantified by using harmonic analysis (Supplemental material Tables 1–3). The results

Fig. 3. Profiles of temperature and cumulative volume concentration of the size-classes: 0–3, 3–10, 10–63, and larger than 63 μm measured at discrete time points (indicated by the box) throughout the 25-h hydrographic survey between 13:00 of Aug. 27 and 14:00 of Aug. 28. The vertical distance is expressed as height above the bed in meters at the time of each profiling. Since *R/V OR-3* does not have a dynamic positioning system, the surveyed water depth at the time of each cast varies slightly (Fig. 1).

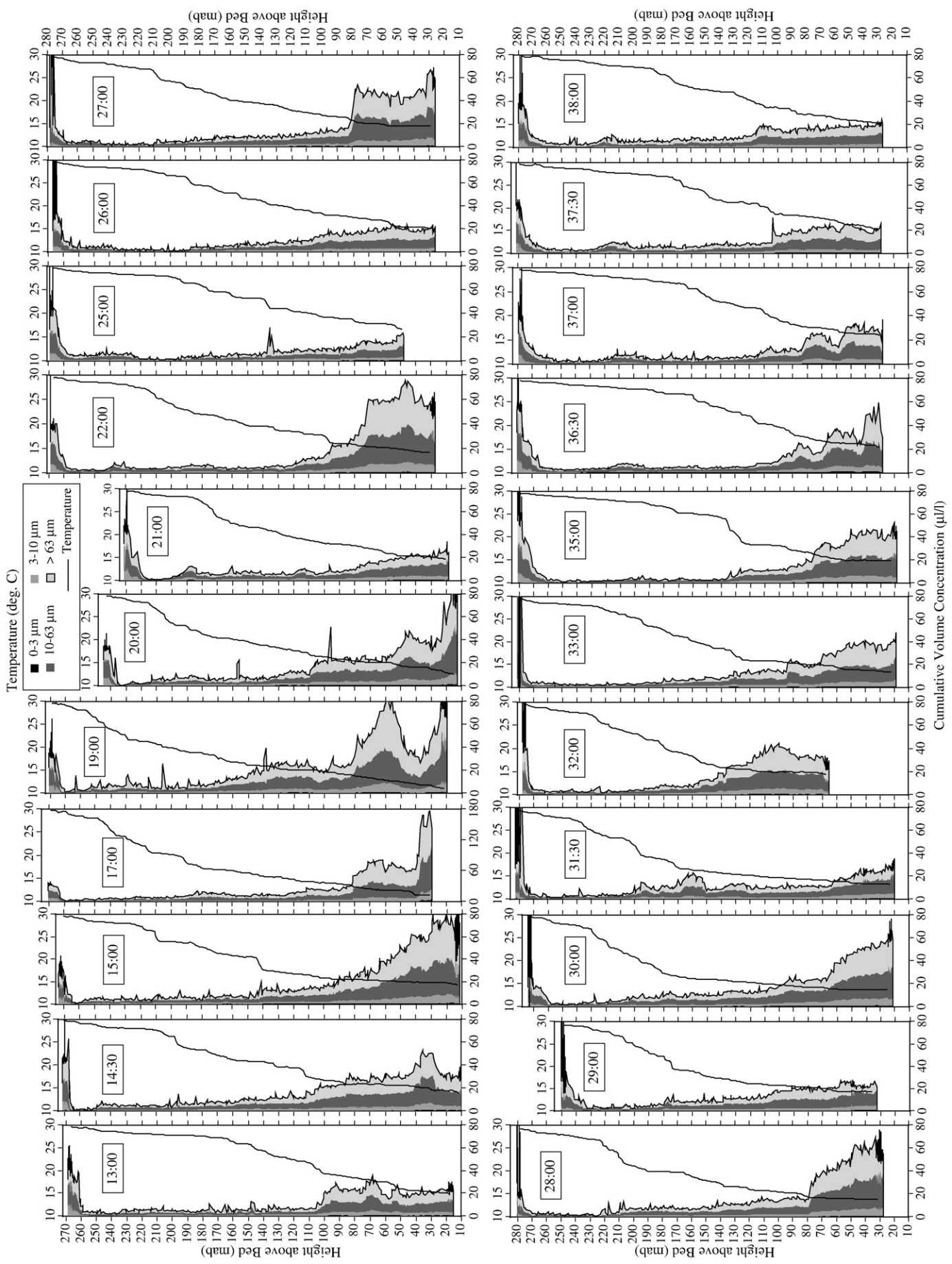
Temperature (deg. C)
0-3 μm
3-10 μm
10-63 μm
> 63 μm
Temperature
Height above Bed (mab)
Cumulative Volume Concentration (μl/l)
13:00
14:30
15:00
17:00
19:00
20:00
21:00
22:00
25:00
26:00
27:00
28:00
29:00
30:00
31:30
32:00
33:00
35:00
36:30
37:00
37:30
38:00

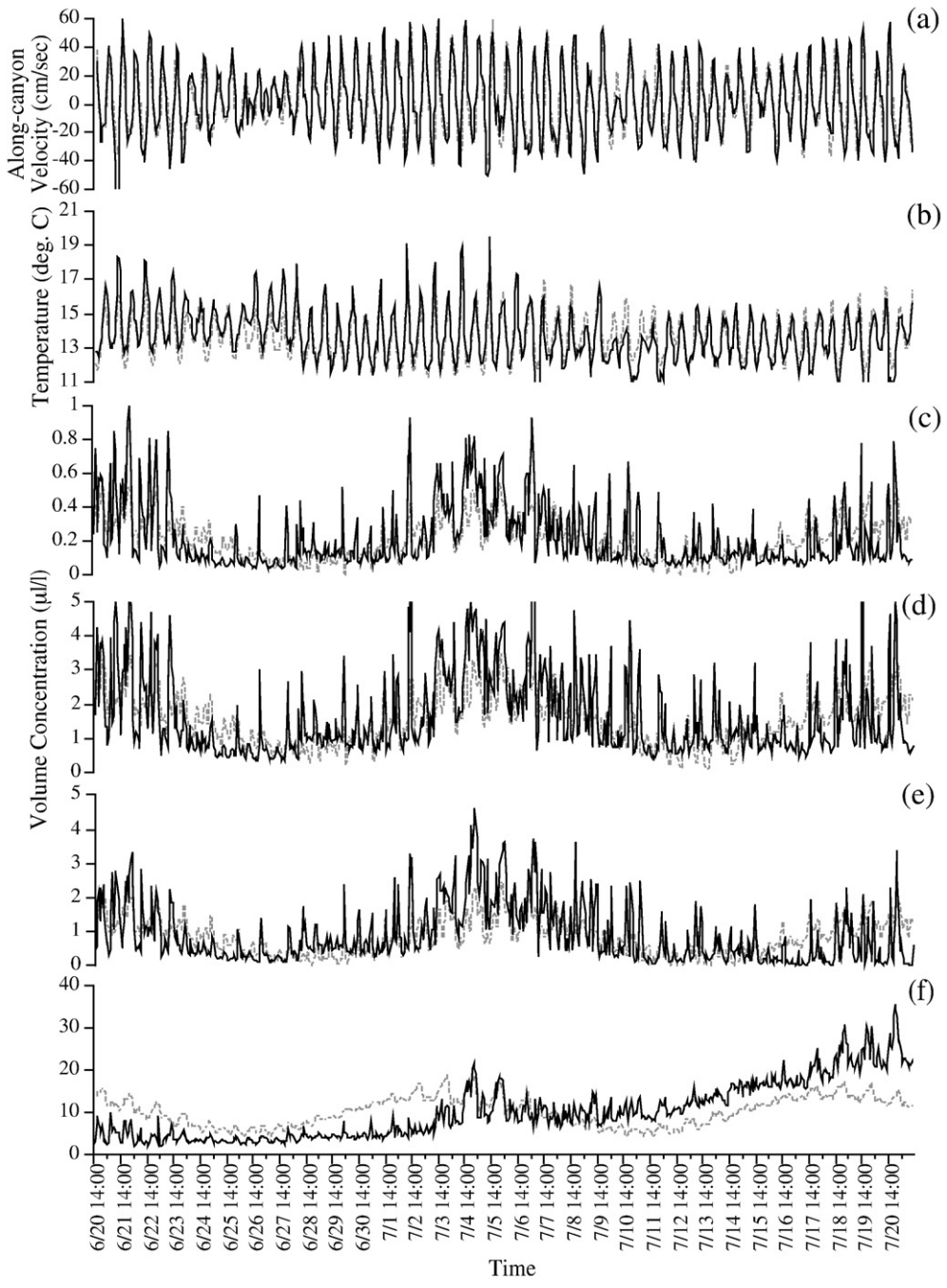

Fig. 4. Month-long instantaneous measurements (solid line) and the tidal hind cast (dashed line) of the along-canyon flow (a); temperature (b); volume concentration of clay (c), very-fine-to-medium silt (d), coarse silt (e), and sand (f) size-classes in 2000.

show that M_2 is the most important semidiurnal constituent and O_1 is the most important diurnal constituent in the KPSC for all the 6 variables examined by this study. Based on the harmonic analysis results of 33 tidal constituents, hind casts of the tidal signals of the along-canyon velocity, water temperature, and the VC of the four size-classes for the duration of the observation were made and plotted with the original data (Figs. 4–6). In each figure, the original record and the hind cast are presented in a descending order: along-canyon velocity (a), water temperature (b), VC of clay (c), very-fine-to-medium silt (d), coarse silt (e), and sand (f), respectively. Although these one-month observations were made in different years, they each encountered a typhoon event (Liu and Lin, 2004; Liu et al. 2006; 2009a).

To compare the characteristic magnitudes of the total and tidal signals of the above time series, the root mean square (RMS) velocity, temperature, and volume concentration of the four size-classes (V_{RMS}) are calculated as follows:

$$V_{RMS} = \left\{ \frac{1}{N} \sum_{i=1}^{N} \left[v(t_i) - \overline{v} \right]^2 \right\}^{1/2} \quad (1)$$

where $v(t_i)$ is the observed variable of instantaneous velocity, temperature, and volume concentration (VC), N is the number of time points in the time series, $\overline{v}$ is the mean value of the time series, (t_i) is the ith time point. The RMS of the tidal signals of each of the 6 variables (T_{RMS}) was subsequently calculated:

$$T_{RMS} = \left\{ \frac{1}{N} \sum_{i=1}^{N} \left[v_p(t_i) - \overline{v} \right]^2 \right\}^{1/2} \quad (2)$$

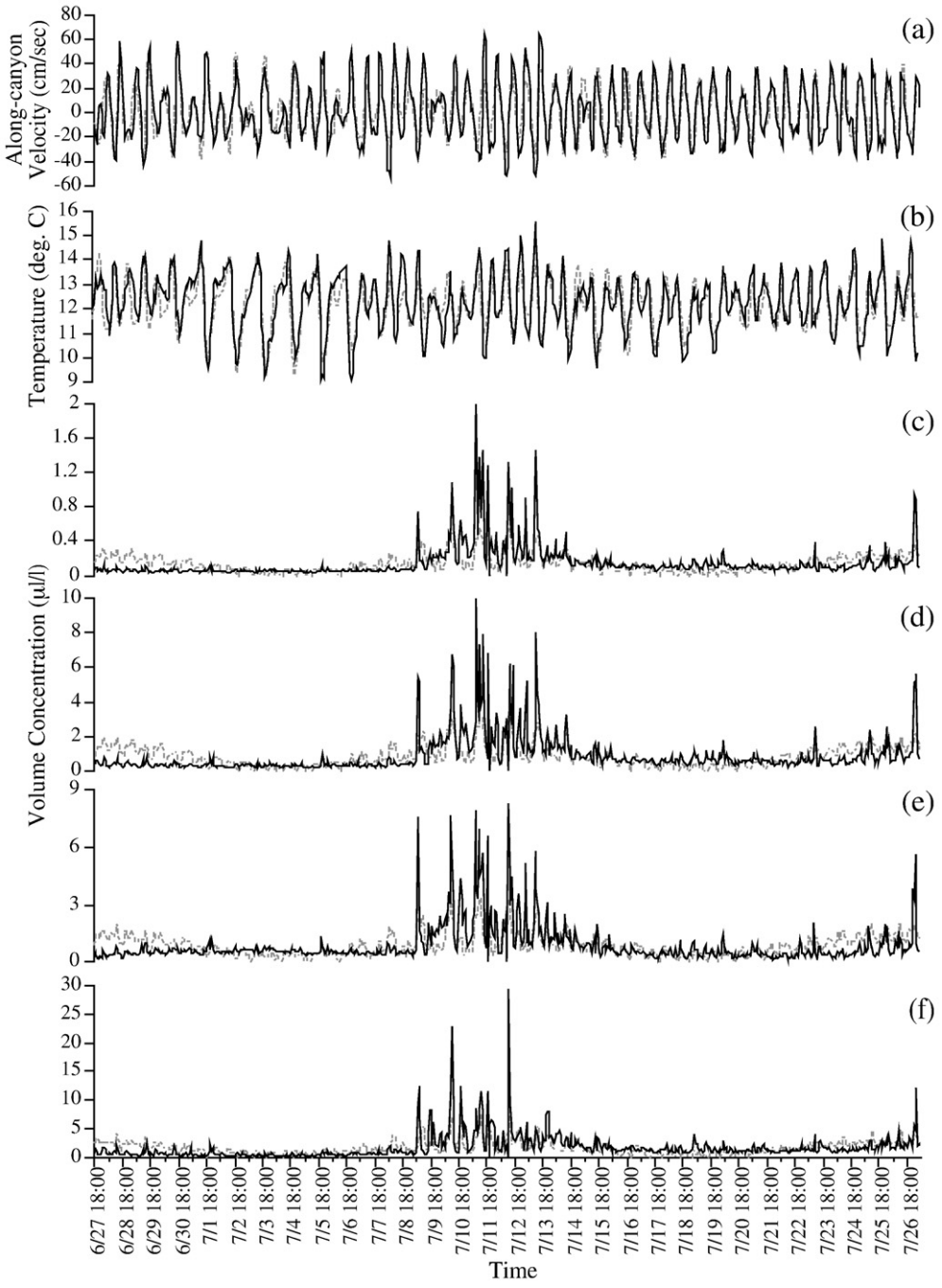

Fig. 5. Month-long instantaneous measurements (solid line) and the tidal hind cast (dashed line) of the along-canyon flow (a); temperature (b); volume concentration of clay (c), very-fine-to-medium silt (d), coarse silt (e), and sand (f) size-classes in 2002.

where $v(t_i)$ is the observed instantaneous values of the variables, $v_p(t)$ = tidal hind cast (synthetic tidal signature) of each time series; and

$$v_p(t) = \sum_{k=1}^{m} a_k \cos(\omega_k t - \theta_k) \tag{3}$$

where $\overline{v}$ = mean value of the observed time series; ω_k = radian frequency ($=2\pi/T_k$); T_k = period of the kth tidal constituent; a_k and θ_k = amplitude and phase, of the kth tidal constituent respectively; and $m=33$.

To further compare the significance of the tide, tidal-to-total energy ratio (ER) for each variable was calculated. The ER is defined as:

$$ER = \frac{\sum\left[v(t_i) - v_p(t_i)\right]^2}{\sum\left[v(t_i) - \overline{v}\right]^2} \times 100\% \tag{4}$$

ER and tidal RMS values of the along-canyon velocity, water temperature, and the VC of the four size-classes are shown in Fig. 7. ER values for the along-canyon flow in 2000 and 2002 were 80% and a little less than 70%, respectively (Fig. 7a). ER value for the flow in 2004 is greater than 90% (Fig. 7a). This is an artificial effect since the harmonic-fit technique was used to rectify the raw data due to the tilt of the moorings (Lee and Liu, 2006). This also explains the small difference between the RMS velocity and RMS tidal velocity in the 2004 data (Fig. 7a). In any case, the RMS tidal flow and total flows near the canyon floor vary between 20 and 24 cm/s.

The temperature records in all the three years are predominantly tidal. The ER values are nearly 100% and there are also very small differences in values between the RMS total and RMS tidal temperatures (Fig. 7b).

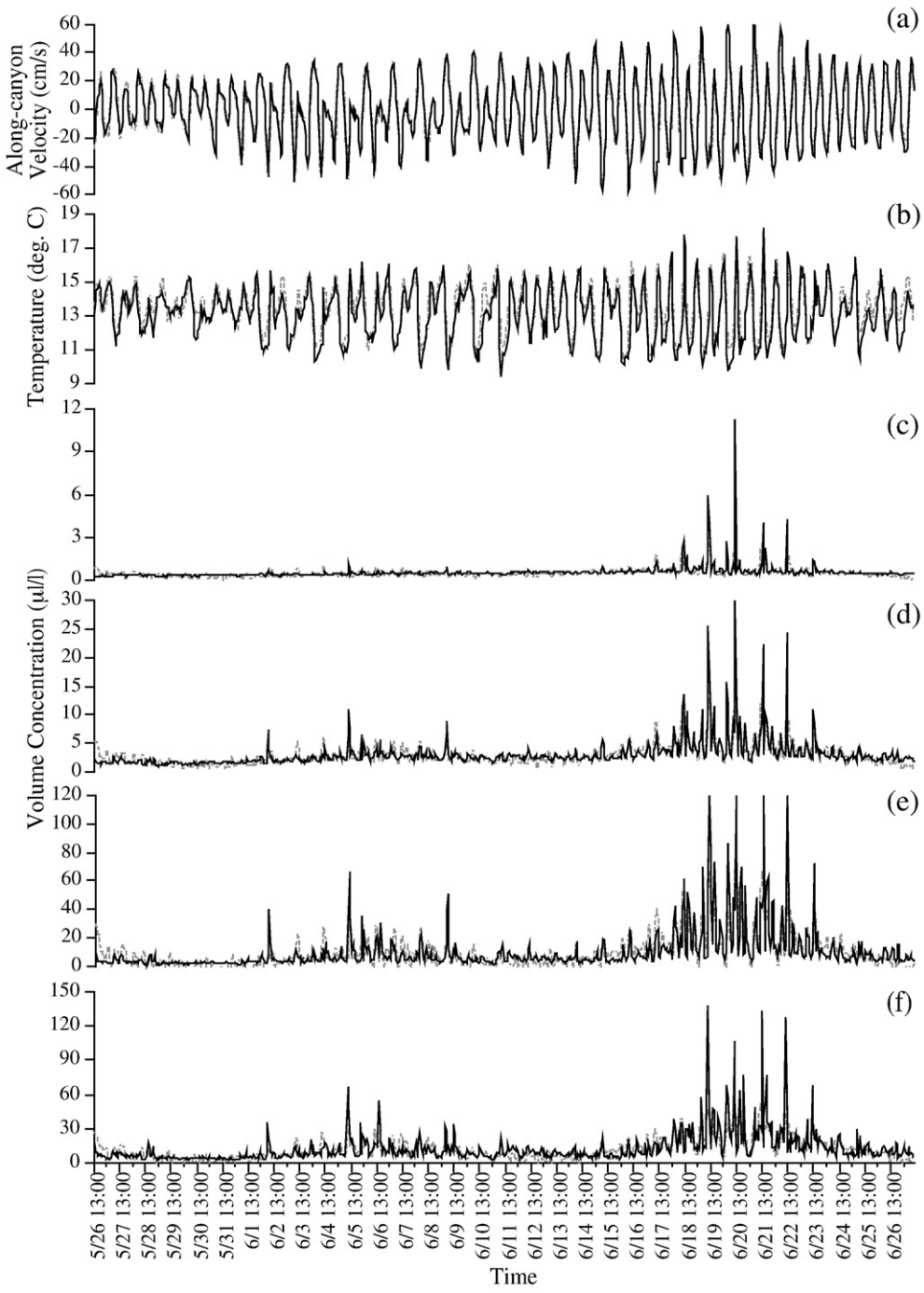

Fig. 6. Month-long instantaneous measurements (solid line) and the tidal hind cast (dashed line) of the along-canyon flow (a); temperature (b); volume concentration of clay (c), very-fine-to-medium silt (d), coarse silt (e), and sand (f) size-classes in 2004.

The tide is also a dominant forcing affecting the temporal variations of the VC in the three record sets. The ER ranges from being a little over 50% to over 80% for different size-classes in different years (Fig. 7c, d, e, f). The RMS VC values and the size-composition of the suspended sediment also varied from year to year. There is usually a 3-order of magnitude difference in the RMS VC values. Usually the clay has the smallest RMS VC values (Fig. 7c), and the sand has the highest VC values (Fig. 7f). Yet in 2004, the coarse silt has the highest RMS values (Fig. 7e). The 2004 RMS VC values are also the highest among all the years. Year 2002 has the lowest ER values for all the VC size-classes, which also have lower RMS values than the other two years.

4.3. Spectral characteristics of measured parameters in the BNL

Based on ER values, although the tide is the most dominant in the temperature, less dominant in the flow, and the least dominant in the VC records; it is helpful to examine the spectral compositions of all the time series records. For each year, the normalized power densities of the along-canyon velocity (shaded) and the temperature (line), and the VC of the 4 size-classes are shown in a descending order (Fig. 8a–e, f–j, k–o).

Visual inspection of these spectra indicates that the energy breakdown of the along-canyon velocity (forcing) by frequency is fairly consistent in the 3 data sets. The most energetic band lies at the semidiurnal frequencies (2 cycles/d). There are four other distinct energy bands at

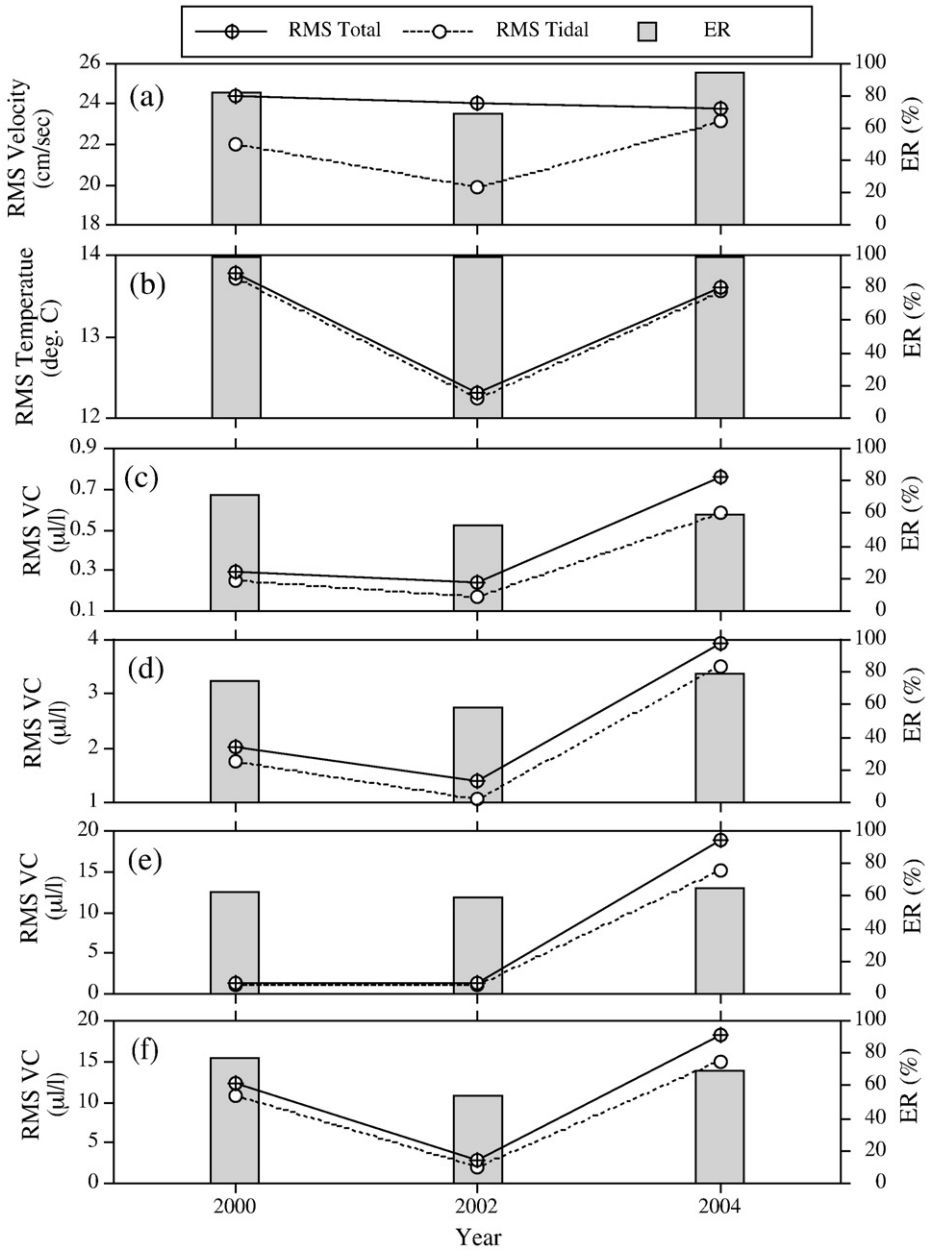

Fig. 7. Tidal-to-total energy ratio (ER) and root mean square (RMS) of total and tidal (a) velocity, (b) temperature, (c) VC of clay, (d) VC of very-fine-to-medium, (e) VC of coarse silt, and (f) VC of sand in 2000, 2002, and 2004, respectively.

the diurnal (1 cpd), third diurnal (3 cpd), fourth diurnal (4 cpd), and subtidal frequencies (less than 0.1 cpd) (Fig. 8a, f, k). Since these frequencies are related to the compound and overtides, their presence suggests nonlinear effects in the submarine canyon flow regime (Pugh, 1987). The last major peak is located at subtidal frequencies, which could be due to the spring-neap tide or other low-frequency forcings. For suspended sediments, the energy at the subtidal frequency band is the highest, suggesting spring-neap and long-term processes are also important factors influencing the temporal fluctuations of suspended sediments in the BNL, which could be related to the season flooding of the Gaoping River or the fluctuations of the Kuroshio branch (Liu et al., 2006).

5. Discussion

5.1. Tide is the predominant forcing causing temporal changes in the BNL

The ER values for all the 6 time series in 3 different years are above 50%, which suggests the tide is the most important forcing that causes the temporal fluctuations in the BNL. In each data set, since the water temperature fluctuation was mainly caused by the tidal advection alone, it has the highest and near 100% ER values (Fig. 7b). Although tidal flow is the major forcing for suspended sediment movements through advection and resuspension, the suspended sediment fluctuations are also subject to the influence of other non-tidal processes such as near-boundary mixing (McPhee-Shaw, 2006), downward settling (Liu et al., 2002) and gravity flows (Liu et al., 2009b). This is why the ER values of VCs are always lower than those of the flow in all the data sets.

When cross-comparing the ER values among the 3 data sets, the year 2002 has the lowest ER values of all variables except the temperature (Fig. 7). The typhoon that occurred in 2002 (from July 8–13) exerted the strongest episodic signal than typhoons in other years such that all the VC values increased by one order of magnitude during this typhoon (Fig. 5, Liu et al., 2006). Due to the large magnitude of pulses during this typhoon, which are non-tidal, the ER values are smaller than those in other years.

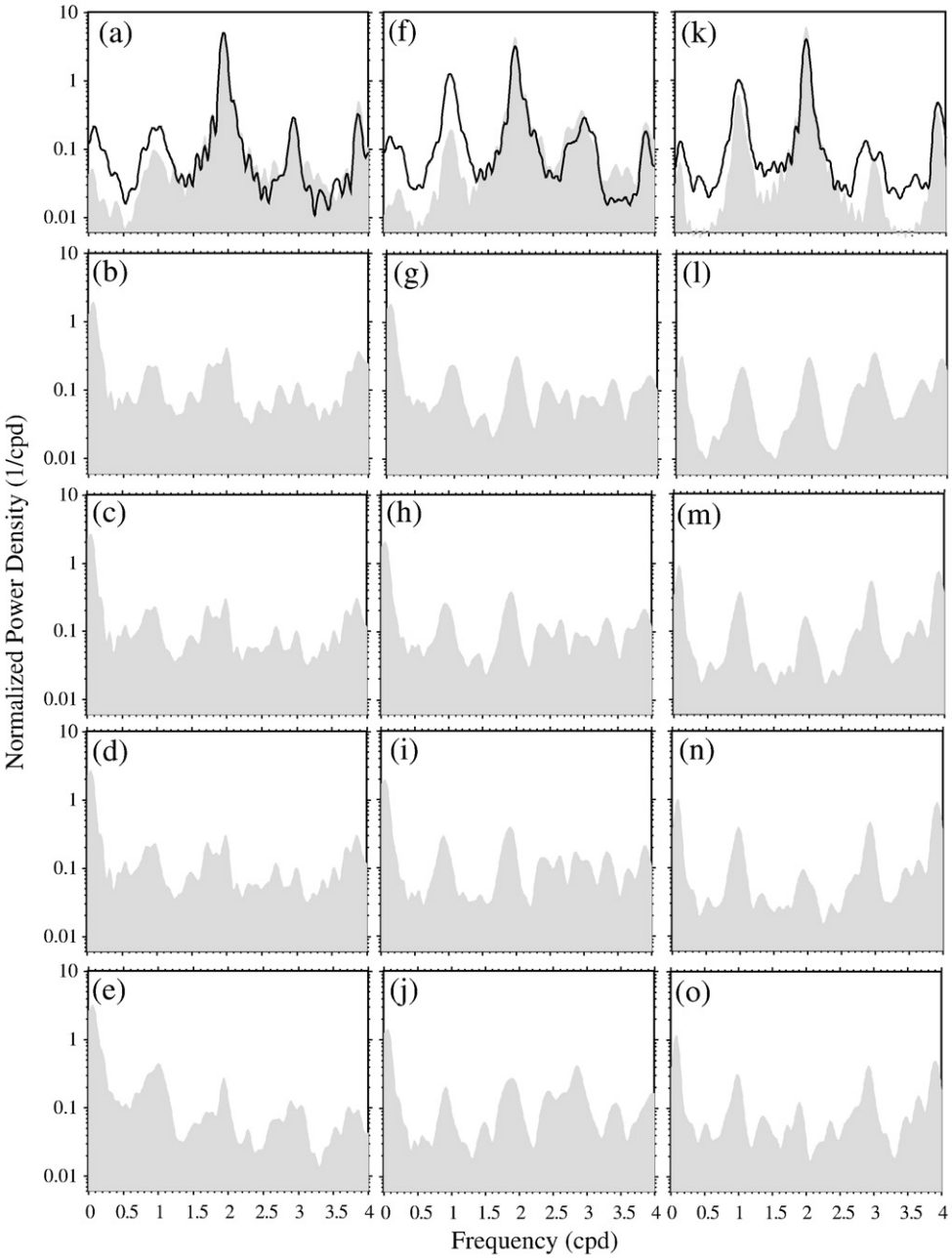

Fig. 8. Normalized power density of the data sets of 2000 (a–e), 2002 (f–j), and 2004 (k–o) by the column showing (a, f, m) along-canyon velocity (shaded region) and temperature (black line) and the VC of clay (b, g, l), very-fine-to-medium silt (c, h, m), coarse silt (d, i, n), and sand (e, j, o), respectively.

5.2. The BNL is closely related to the propagation of the semidiurnal internal tide in the canyon

In the course of a semidiurnal tidal cycle, the advection of colder offshore water that contains a higher concentration of suspended sediment causes the thickness of BNL to increase and decrease at the semidiurnal frequency (Fig. 3). The displacement of the top of the BNL is on the same order of hyperpycnal surface displacement due to the nonlinear internal tide, or barotropic tide (Lee et al., 2009a; Wang et al., 2008), or the reflection of the semidiurnal internal tide (McPhee-Shaw, 2006). The phase differences at the M_2 frequency among the along-canyon flow and the temperature, VC of clay, very-fine-to-medium silt, coarse silt, and sand indicate two different patterns of phase-locking. The 2002 and 2004 data sets have similar patterns in which a phase difference between 90 and 110° exists (Fig. 9). This is indicative of the existence of the standing semidiurnal internal tide (Lee et al., 2009b, Wang et al., 2008) that causes the vertical displacement of water mass as well as the resuspension of bottom sediments.

The phase lag for 2000 displays a different pattern. The 90–110-degree phase difference between the current and water temperature also indicates the displacement of water mass by the internal tidal current. However, the around-zero phase difference between the flow and the VC of the 4 suspended sediment size-classes indicates that the suspended sediment fluctuations in the BNL are associated with the horizontal advection. The in phase relations of the flow and sediments are also shown in the time series plot (Fig. 4) that high sediment concentrations occurred frequently at strong currents. It is speculated that since the 2000 mooring was the closest to the canyon wall, the complex canyon cross-section morphology caused the displacement of water mass and the advection of suspended sediments to be influenced by different processes.

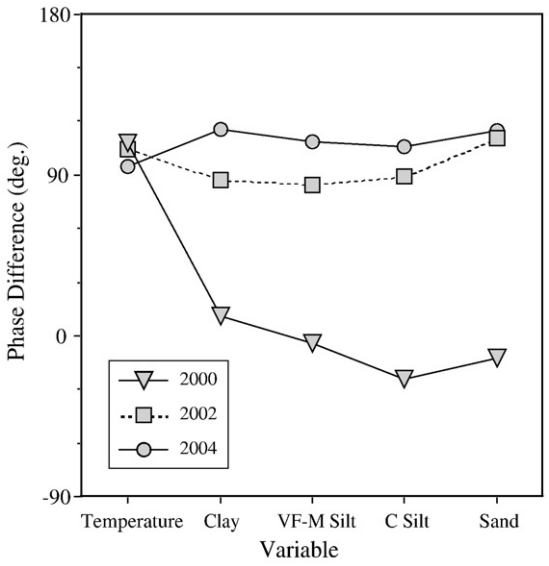

Fig. 9. Phase difference (local phase) of the along-canyon velocity minus that of the clay, very-fine-to-medium silt, coarse silt, and sand at the M_2 frequency for the three years.

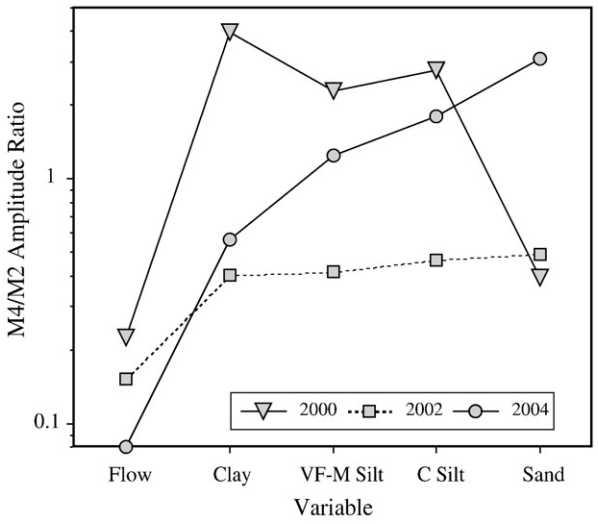

Fig. 10. The M_4/M_2 amplitude ratio of the along-canyon velocity, clay, very-fine-to-medium silt, coarse silt, and sand for 2000, 2002, and 2004, respectively.

In either pattern, the phase-locking between suspended sediment size-classes and the tidal flow suggests that the suspended sediment, despite of their grain sizes, respond to the dominant M_2 forcing in a site-specific and yet coherent way in the BNL.

5.3. Suspended sediment movements in the BNL are nonlinear

Over a semidiurnal tidal cycle elevated suspended sediment concentrations are corresponding to the entrainment by the shear stress induced by max. flood and ebb flows in the BNL (Fig. 2), which is a nonlinear process dictated by the quadratic stress law. Overtides and compound tides in all VC time series are also resolved by the harmonic analysis (Supplemental material Tables 1–3). It is clear that the suspended sediment transport in the BNL is related to nonlinear processes. A direct measure of nonlinearity generation is the amplitude ratio between the M_2 and its overtide M_4 (M_2/M_4), which is the first harmonic (Aubrey and Friedrichs, 1988; McPhee-Shaw, 2006; Parker, 1991).

The results show a great diversity in the 3 data sets. Across the canyon, the 2004 mooring is located in the thalweg and the 2000 and 2002 moorings are positioned away from the thalweg towards the canyon wall (Fig. 1). There is an inverse relationship between the M_2/M_4 ratio of the flow and the distance to the canyon wall such that the closer to the canyon wall, the higher the M_2/M_4 ratio (Fig. 10). This suggests the boundary effect of the wall on the nonlinearity generation in the flow.

However, the M_2/M_4 ratios of all the 4 size suspended sediments are all higher than that of the flow (Fig. 10). This indicates that the suspended sediments in the BNL are subject to a greater set of nonlinear processes than the flow. Yet, there is diversity in the values of the ratio among different grain-size-classes even in the same year except for 2002. Since the 2002 mooring is located in a relative open spot in the canyon, it is probably less affected by boundary-related mixing and entrainment processes and thus, all size-classes have a uniform value of M_2/M_4 ratio. As for the other two years, it is not clear what size-specific nonlinear processes are causing the different M_2/M_4 ratios.

5.4. Topographic effect on the propagation of internal tides that effect the BNL

The topography, which includes canyon cross-section geometry and the slope of the canyon floor, affects the propagation of internal tides, which in turn, affects the energy dissipation and nonlinearity generation. The 2002 and 2004 moorings are located on the south side of the canyon meander (Fig. 1), which is in the path of up-canyon propagating barotropic and internal tides. The reflected and incoming tides easily form standing waves and this explains the standing wave characteristics in the BNL measured by the 2002 and 2004 moorings. At the 2000 mooring site progressive waves are more influential on the transport of suspended sediments (indicated by near-zero degree phase lag with the flow) and yet, the advection of water masses is affected by the standing internal wave (indicated by the near 90-degree phase lag with the flow, Fig. 9).

Because of the earth's rotation, the cross-canyon distribution of the internal tidal energy favors the right-hand side in the direction of propagation in the northern hemisphere (Petruncio et al., 2002). In our case, it is the southeast side of the canyon meander where the moorings were deployed. Additionally, secondary flow cells in meandering submarine channels are best developed at the bend apex with the basal component of the flow moving from the inside to the outside of the bend (Keevil et al., 2006). The secondary flow also promotes higher levels of turbulence. The combination of the secondary flow that upwells at the outer band (in our case, the canyon wall) provides a mechanism for the formation of coarser deposits on the outer bank bend (Keevil et al., 2006). In our case, it is also from the west side (2000 mooring) to the east side (2004 mooring) at the mooring sites (Fig. 1). This could explain the highest VCs and increasing nonlinearity with grain size (Fig. 10) observed by the 2004 mooring. The cross-canyon flow asymmetry and secondary flow cell could generate lateral transport (Wang et al., 2008) that also contributes to the differences among the observations of the three moorings.

6. Conclusion

The characteristics of the BNL in the KPSC, including its thickness, flow, water temperature, and the concentrations of suspended sediments of different grain sizes, possess distinctive tidal signatures. The semidiurnal internal tide at the M_2 frequency is the most dominant forcing that causes major fluctuations in the NBL. Temporal changes of the suspended sediment in the BNL are related to nonlinear processes that are also influenced by the geometry of the canyon cross-section, the slope of the canyon, and the proximity to the canyon wall.

Acknowledgements

The funding for this study was provided by the R.O.C. National Science Council under grant numbers NSC91-2611-M-110-017, NSC92-2611-M-110-012, NSC93-2611-M-110-013, NSC94-2611-M-110-002, NSC 95-2611-M-110-018 and NSC 96-2611-M-110-010. We thank the captain and crew of the *R/V OR-3* for their service. We are indebted to the staff of the Sediment Trap Laboratory of the Taiwan Ocean Research Institute for the design, construction, deployment, and retrieval of sediment trap moorings. We are grateful to Jeff C. Huang, and Fanta Hsu for their help in the fieldwork and Tony Hsu for data and analysis. Marilyn Ritzer-Liu proofread a later version of the manuscript.

Appendix A. Supplementary data

Supplementary data associated with this article can be found, in the online version, at doi:10.1016/j.margeo.2010.01.016.

References

Aubrey, D.G., Friedrichs, C.T., 1988. Seasonal climatology of tidal non-linearities in a shallow estuary. In: Aubrey, D.G., Weishar, L. (Eds.), Hydrodynamics and Sediment Dynamics of Tidal Inlets. Springer-Verlag, New York, pp. 103–124.

Chronis, G., Georgopoulos, L.D., Zervakis, V., Stavrakakis, S., Poulos, S., 2000. Suspended particulate matter and nepheloid layers over the southern margin of the Cretan Sea (N.E. Mediterranean): seasonal distribution and dynamics. Progress in Oceanography 46, 163–185.

Frignani, M., Courp, T., Cochran, J.K., Hirshberg, D., Codina, L.V. i, 2002. Scavenging rates and particle characteristics in and near the Lacaze–Duthiers Submarine Canyon, Northwest Mediterranean. Continental Shelf Research 22, 2175–2190.

Forest, A., Sampei, M., Hattori, H., Makabe, R., Sasaki, H., Fukuchi, M., Wassmann, P., Fortier, L., 2007. Particulate organic carbon fluxes on the slope of the Mackenzie Shelf (Beaufort Sea): physical and biological forcing of shelf-basin exchanges. J. Mar. Syst. 68, 39–54.

Inthorn, M., Mohrholz, V., Zabel, M., 2006. Nepheloid layer distribution in the Benguela upwelling area offshore Namibia. Deep-Sea Res. 53, 1423–1438.

Johnson, D.N., Weidemann, A., Pegau, W.S., 2001. Internal tidal bores and bottom nepheloid layers. Cont. Shelf Res. 21, 1473–1484.

Karageorgis, A.P., Anagnostou, C.L., 2001. Particulate matter spatial-temporal distribution and associated surface sediment properties: Thermaikos Gulf and Sporades Basin, NW Agean Sea. Cont. Shelf Res. 21, 2141–2153.

Keevil, G.M., Peakall, J., Best, J.L., Amos, K.J., 2006. Flow structure in sinuous submarine channels: velocity and turbulence structure of an experimental submarine channel. Mar. Geol. 229, 241–257.

Kunze, E., Rosenfeld, L.K., Carter, G.S., Gregg, M.C., 2002. Internal waves in Monterey Submarine Canyon. J. Phys. Oceanogr. 32, 1890–1913.

Lee, I.-H., Liu, J.T., 2006. Rectification of the heading and tilting of sediment trap arrays due to strong tidal currents in a submarine canyon. Geophys. Res. Lett. 33, L08609. doi:10.1029/2005GL025183.

Lee, I.-H., Lien, R.-C., Liu, J.T., Chuang, W.-S., 2009a. Turbulent mixing and internal tides in Gaoping (Kaoping) Submarine Canyon, Taiwan. J. Mar. Syst. 76 (4), 383–396.

Lee, I.-H., Wang, Y.-H., Liu, J.T., Chuang, W.-S., Xu, J.P., 2009b. Internal tidal currents in the Gaoping (Kaoping) Submarine Canyon. J. Mar. Syst. 76 (4), 397–404.

Liu, J.T., Liu, K.-j, Huang, J.C., 2002. The influence of a submarine canyon on river sediment dispersal and inner shelf sediment movements: a perspective from grain-size distributions. Mar. Geol. 181, 357–386.

Liu, J.T., Lin, H.-L., 2004. Sediment dynamics in a submarine canyon: a case of river-sea interaction. Mar. Geol. 207, 55–81.

Liu, J.T., Lin, H.-L., Hung, J.-J., 2006. A submarine canyon conduit under typhoon conditions off Southern Taiwan. Deep-Sea Res. 53, 223–240.

Liu, J.T., Hung, J.-J., Lin, H.-L., Huh, C.-A., Lee, C.-L., Hsu, R.T., Huang, Y.-W., Chu, J.C., 2009a. From suspended particles to strata: the fate of terrestrial substances in the Gaoping (Kaoping) Submarine Canyon. J. Mar. Syst. 76 (4), 417–432.

Liu, J.T., Huh, C.-A., You, C.-F., 2009b. Fate of terrestrial substances in the Gaoping (formerly spelled Kaoping) Submarine Canyon. J. Mar. Syst. 76 (4), 367–368.

Masque, P., Fabres, J., Canals, M., Sanchez-Cabez, J.A., Sanchez-Vidal, A., Cacho, I., Calafat, A.M., Bruach, J.M., 2003. Accumulation rates of major constituents of hemipelagic sediments in the deep Alboran Sea: a centennial perspective of sedimentary dynamics. Mar. Geol. 193, 207–233.

McCave, I.N., Hall, I.R., Antia, A.N., Chou, L., Dehairs, F., Lampitt, R.S., Thomsen, L., van Weering, T.C.E., Wollast, R., 2001. Distribution, composition and flux of particulate material over the European margin at 47°–50° N. Deep-Sea Res. II 48, 3107–3139.

McCave, I.N., Hall, I.R., 2002. Turbidity of waters over the Northwest Iberian Continental Margin. Prog. Oceanogr. 52, 299–313.

McPhee-Shaw, E., 2006. Boundary-interior exchange: review the idea that internal-wave mixing enhances lateral dispersal near continental margins. Deep-See Research II 53, 42–59.

McPhee-Shaw, E.E., Sternberg, R.W., Mullenbch, B., Ogston, A.S., 2004. Observations of intermediate nepheloid layers on the Northern California continental margin. Cont. Shelf Res. 24, 693–720.

Oliveira, A., Vitorino, J., Rodrigues, A., Jouanneau, J.M., Dias, J.A., and Weber, O., 2002. Nepheloid layer dynamics in the northern Portuguese shelf. Progress in Oceanography, 52, 195–213. Wang, Y.H., Lee, I.H., and Liu, J.T., 2008. Observation of internal tidal currents in the Kaoping Canyon off southwestern Taiwan. *Estuarine, Coastal and Shelf Science*, 80(1), 153–160.

Oliveira, A., Santos, A.I., Rodrigues, A., Vitorino, J., 2007. Sedimentary particle distribution and dynamics on the Nazare Canyon system and adjacent shelf (Portugal). Mar. Geol. 246, 105–122.

Parker, B.B., 1991. The relative importance of the various nonlinear mechanisms in a wide range of tidal interactions (review). In: Parker, B.B. (Ed.), Tidal Hydrodynamics. John Wiley and Sons, Inc., New York, pp. 237–268.

Petruncio, E., Paduan, J.D., Rosenfeld, L.K., 2002. Numerical simulations of the internal tide in a submarine canyon. Ocean Modeling 4, 221–248.

Pugh, D.T., 1987. Tides, surges, and mean sea-level. John Wiley and Sons, New York. 472p.

Puig, P., Palanques, A., 1998. Nepheloid structure and hydrographic control on the Barcelona continental margin, Northwestern Mediterranean. Mar. Geol. 149, 39–54.

Puig, P., Palanques, A., Guillen, J., 2001. Near-bottom suspended sediment variability caused by storms and near-inertial internal waves on Ebro mid continental shelf (NW Mediterranean). Mar. Geol. 178, 81–93.

Puig, P., Palanques, A., Guillen, J., El Khatab, M., 2004. Role of internal waves in the generation of nepheloid layers on the Northwestern Alboran Slope: implications for continental margin shaping. J. Geophys. Res. 109, C09011. doi:10.1029/2004JC002394.

Ramaswamy, V., Rao, P.S., Rao, K.H., Thwin, S., Rao, N.S., Raiker, V., 2004. Tidal influence on suspended sediment distribution and dispersal in the Northern Andaman Sea and Gulf of Martaban. Mar. Geol. 208, 33–42.

Ribbe, J., Holloway, P.E., 2001. A model of suspended sediment transport by internal tides. Cont. Shelf Res. 21, 395–422.

van der Loeff, M.M.R., Meyer, R., Rudels, B., Rachor, E., 2002. Rususpension and particle transport in the benthic nepheloid layer in and near Fram Strait in relation to faunal abundances and 234th depletion. Deep-Sea Res. 49, 1941–1958.

van Weering, T.C.E., De Stigter, H.C., Balzer, W., Epping, E.H.G., Graf, G., Hall, I.R., Helder, W., Khripounoff, A., Lohse, L., McCave, I.N., Thomsen, L., Vangriesheim, A., 2001. Benthic dynamics and carbon fluxes on the NW European continental margin. Deep-Sea Res. II 48, 3191–3221.

Vitorino, J., Oliveira, A., Jouanneau, J.M., Drago, T., 2002. Winter dynamics on the Northern Portuguese Shelf. Part 2: Bottom boundary layers and sediment dispersal. Prog. Oceanogr. 52, 155–170.

Wang, Y.H., Lee, I.H., Liu, J.T., 2008. Observation of internal tidal currents in the Kaoping Canyon off Southwestern Taiwan. Estuar. Coast. Shelf Sci. 80 (1), 153–160.

Yurkovskis, A., 2005. Seasonal benthic nepheloid layer in the Gulf of Riga, Baltic Sea: sources, structure and geochemical interactions. Cont. Shelf Res. 25, 2182–2195.

Zhu, Y.Z., Zhang, J., Wu, Y., Lin, J., 2006. Bulk particulate organic carbon in the East China Sea: tidal influence and bottom transport. Prog. Oceanogr. 69, 37–60.